Modeling and dynamic characteristic simulation of air-cooled proton exchange membrane fuel cell stack for unmanned aerial vehicle

Chengyuan Gong[a], Lu Xing[b,*], Cong Liang[c, d], Zhengkai Tu[a,*]

[a] School of Energy and Power Engineering, Huazhong University of Science and Technology, Wuhan, 430074, China

[b] Mechanical and Construction Engineering, Northumbria University, Newcastle upon Tyne, NE1 8ST, United Kingdom

[c] China Automotive Technology and Research Center Co., Ltd., No.68 East Xianfeng Road, Tianjin, China

[d] CATARC Automotive Test Center (Wuhan) Co., Ltd., No.55 Zhuanyang Avenue, Wuhan, China

*Corresponding author:

Lu Xing, lu.xing@northumbria.ac.uk;

Zhengkai Tu, tzklq@hust.edu.cn.

Fax: +86 27 87540724

Tel.: +86 (0) 2787542618

Abstract

Air-cooled low-temperature proton exchange membrane fuel cell stack applied with metallic bipolar plate is considered as a promising power source for an unmanned aerial vehicle. This paper presents a coupled electrochemical thermal model for simulating its dynamic characteristic. The impact of the applied metallic bipolar plate on the stack thermal balance is considered; an environmental model estimating atmospheric temperature and pressure variations with altitude is included. Our theoretical analysis shows that with altitude increased from 0m to 4000m, the output electric power declined rate is 4.7-6.5% at the current density of 400-800 $mA \cdot cm^{-2}$. To avoid severe stack degradation due to high stack operating temperature, minimum air stoichiometric ratio is required for maintaining stack thermal balance. When the altitude increases from 0 to 4000m, the minimum required air stoichiometric ratio decreases from 110 to 22 at the current density of 800 $mA \cdot cm^{-2}$.

Keywords: Proton exchange membrane fuel cell; Air-cooled; Performance; Thermal management; Unmanned aerial vehicle

1. Introduction

Proton exchange membrane fuel cell (PEMFC) has been widely applied all over the industrial and commercial fields, due to its low operation temperature, high power/mass ratio, fast response, no emission and low noise [1, 2]. It can be used for combined heat and power generation [3, 4], for automobiles industry [5-8] and for unmanned aerial vehicles (UAVs) [9, 10]. The low-temperature PEMFC stack for UAV is preferred to be applied with metallic bipolar plate and to be air cooled because of severe restrictions for weight and space available [11].

Fuel cell stack made of metallic bipolar plates weighed much less than a fuel cell stack made of carbon graphite [12, 13]. Furthermore, stainless steel bipolar plates have better electrical and thermal conductivity, higher shock resistance and higher gas barrier properties compared with graphite bipolar plates [14, 15]. Considerable efforts focusing on the surface coating [16-18] or on flow channel optimization [19-21] have been made to optimize the design of bipolar plates. These researches focus on liquid-cooled stack, while there are few researches on air-cooled stack applied to UAV. Other materials like polymers also have been used in bipolar plates which are suitable for compression molding, transfer molding, or injection molding [22]. However, studies mentioned above have been mainly conducted in stationary and laboratory settings, where vibration intensity and lightweight are not critical. The metallic bipolar plates have the advantage of vibration-resistant, firm structure, light weight [23] which can withstand harsh and uncertain environments effectively. Therefore, the metallic bipolar plate is

more suitable for UAV.

The dynamic performance and thermal management of the air-cooled PEMFC stack are crucial for the UAV since both of them concern efficiency optimization and fuel cell life span, especially for mission success. For PEMFC powered UAV, the atmospheric temperature, atmospheric pressure, and oxygen partial pressure will change with the variation of altitude during the operation of UAV. Altitude variations can lead to the stack performance degradation and bring challenges for thermal management. Therefore, theoretical analysis of altitude variations influence on stack operational performance and thermal management is critical and necessary to be performed.

Electrochemical models for steady state and dynamic characteristic simulations of the PEMFC have been developed over the years. Mann et al. [24] established a generalized steady-state electrochemical model for a PEMFC. Thermodynamic potential, the activation overvoltage and the ohmic overvoltage were included in this expression. Musio et al. [25] constructed a validated and modular model of a PEMFC stack which includes the concentration overvoltage in the fuel cell voltage formula, a good match with experimental data was observed in their results. Seleem et al. [26] proposed a novel and simplified precise model for the PEMFCs. The unknown model parameters were reduced to four and could be obtained using the metal-heuristic algorithm (or called equilibrium optimizer). Khan and Iqbal [27] discussed dynamic modeling and simulation methods for a PEMFC system, it reflected various features arising due to transients in cell electrochemistry, energy balance and reactant flow. Zhang et al. [29]

developed a control-oriented thermal model for the air-cooled PEMFC and proposed a model predictive control-based temperature regulation strategy. The temperature characteristics of the open-cathode PEMFC can be effectively described by the developed models and the better performance could be obtained comparing to the traditional PI controller.

Some researches focused on the fuel cell hybrid propulsions systems in UAV, fuel cells with other power sources such as batteries [30, 31], super capacitors [13], and solar cells [32]. Depcik et al. [33] compared the UAV powered by lithium-ion batteries, hydrogen fueled combustion engines and the fuel cell. The results showed that a Li-air battery pack would have the longest flight time and simplest configuration. Gonzalez-Espasandin [34] investigated the direct methanol fuel cell (DMFC) and PEMFC performance under flight conditions for the UAV. Renau et al. [35] presented the design of high-temperature PEMFC and its cooling system to power a UAV for a high-altitude mission. The design, manufacture and operational tests of a lightweight HT-PEMFC were optimized. Horde et al. [36] studied the sensitivity to altitude using experimental data and a developed electrochemical model, at three different altitudes 200, 1200 and 2200m. Results indicated that the fuel cell power decreased as the altitude increased.

So far, the coupled electrochemical and thermal model for the PEMFC stack of a UAV applied with metallic bipolar plate has not been developed. The dynamic characteristic simulation considering influences of altitude variations has not been performed. In this paper, we propose an electrochemical model and a thermal model for the air-cooled

PEMFC stack of a UAV. The impact of the applied metallic bipolar plate on the stack thermal balance and an environmental model estimating atmospheric temperature and pressure variations with altitude are included. Theoretical analysis for the influence of altitude variations on stack operational performance and thermal management has been carried out. Fan supplies cathode intake air, meanwhile, the air flow removes waste heat to maintain stack thermal balance. We also investigate influence of air stoichiometric ratio on the thermal performance of the PEMFC stack.

2. Methodology

A coupled electrochemical and thermal model is proposed for the simulation of air-cooled PEMFC stack of an UAV. An environmental model which considers the atmospheric temperature and pressures changes due to the altitude variations is integrated with the coupled electrochemical and thermal model. The electrochemical model has been validated against experimental data. The cell temperature is affected by the environment (pressure, ambient temperature) and load, the output power of the cell will be in turn affected by the cell temperature. Therefore, this is a complex coupling process for the performance of a single cell. The heat transfer and heat generation process between numerous single cells forms the temperature distribution in an PEMFC stack.

2.1. Electrochemical model

The PEMFC stack uses hydrogen as a fuel and oxygen (in the ambient air) as an oxidant,

121 continuously outputs electrical energy through an electrochemical reaction. The
122 electrochemical model is developed based on method proposed by Jia et al. [37],
123 detailed information of empirical parameters for the model equations are also presented
124 by Khan and Iqbal [27]. The output voltage of fuel cell can be obtained considering
125 ohmic loss, concentration loss and activation loss in the fuel cell stack, as shown in
126 Equation (1):

127 $$V_{\text{cell}} = E_{\text{nernst}} - V_{\text{ohmic}} - v_{\text{d}} \quad (1)$$

128 Where, V_{cell} is the single fuel cell voltage (V). V_{ohm} is the ohmic loss (V) due to the
129 impedance of transmission. v_{d} is the overall voltage drop because of concentration
130 loss and activation loss, it will be calculated using the equivalent circuit model and
131 explained in detail in section 2.1.1. E_{nernst} is the Nernst open circuit voltage (V) can
132 be expressed as a function of fuel cell operating temperature, partial pressures of
133 hydrogen and oxygen in the fuel cell as shown in Equation (2):

134 $$E_{\text{nernst}} = \frac{1}{2F}(\Delta G - \Delta S(T - T_{ref}) + \frac{RT}{2F}\ln(P_{\text{H}_2}(P_{\text{O}_2})^{0.5}) \quad (2)$$

135 The ohmic overvoltage V_{ohmic} can be calculated with Ohm's law as shown in Equation
136 (3):

137 $$V_{\text{ohmic}} = I_{\text{cell}}(R_{\text{M}} + R_{\text{c}}) \quad (3)$$

138 Where, I_{cell} is the cell current (A). R_{c} is the contact resistances both between the
139 membrane and electrodes as well as the electrodes and the bipolar plates (Ω). R_{M} is
140 the equivalent membrane impedance (Ω) as shown in Equation (4) [37]:

$$R_{\mathrm{M}} = \frac{r_{\mathrm{M}} l_{\mathrm{mem}}}{A}$$

$$r_{\mathrm{M}} = \frac{181.6\left[1+0.03\left(\frac{I}{A}\right)+0.062\left(\frac{T}{303}\right)^{2}\left(\frac{I}{A}\right)^{2.5}\right]}{\left[\lambda-0.634-3\left(\frac{I}{A}\right)\right]\exp\left(4.18\frac{(T-303)}{T}\right)} \quad (4)$$

2.1.1. Equivalent circuit model

There is a 'double layer capacitance' phenomenon in PEMFC [38] as shown in Fig. 1. An electrical capacitor can be considered as the layer of charge on or near the electrode–electrolyte interface [37]. They act as charge and energy storage devices, which are equivalent to a capacitor. This phenomenon will impact the activation and concentration losses. The ohmic overvoltage will not be affected. The activation losses can be computed according to the empirical equation as shown in Equation (5) [37]:

$$V_{\mathrm{act}} = \xi_1 + \xi_2 T + \xi_3 T\left[\ln\left(C_{\mathrm{O}_2}\right)\right] + \xi_4 T[\ln(I)]$$
$$\xi_1 = -0.948$$
$$\xi_2 = 0.00286 + 0.0002\ln(A) + 4.3\times10^{-5}\ln\left(C_{\mathrm{H}_2}\right) \quad (5)$$
$$\xi_3 = 7.6\times10^{-5}$$
$$\xi_4 = -1.93\times10^{-4}$$

Where C_{H_2} is the hydrogen concentration at the anode/membrane interface. The reactant concentrations at the electrode/membrane interfaces could be determined by Henry's law [24]:

$$C_{\mathrm{O}_2} = P_{\mathrm{O}_2}\times1.97\times10^{-7}\exp\frac{498}{T}$$
$$C_{\mathrm{H}_2} = P_{\mathrm{H}_2}\times9.174\times10^{-7}\exp\frac{-77}{T} \quad (6)$$

The concentration loss is needed to be included because of high concentration loss at high current density regime. The concentration loss can be expressed as [35]:

$$V_{\mathrm{con}} = \frac{RT}{2F}\ln\left(1-\frac{i}{i_{\max}}\right) \quad (7)$$

As shown in Fig. 1 (a), at the surface of the fuel cell cathode, a simple equivalent circuit

158 model of the PEMFC in which an electrical capacitor can be considered as the layer of
159 charge on or near the electrode-electrolyte interface as shown in Fig. 1 (b) [37-39]. The
160 voltage at both ends of the equivalent capacitor varies dynamically with the current
161 until the voltage reaches the next steady value. The process can be expressed as
162 Equation (8):

163 $$\frac{dv_{\mathrm{d}}}{dt} = \frac{I_{\mathrm{cell}}}{C} - \frac{v_{\mathrm{d}}}{\tau} \tag{8}$$

164 Where, t is time (s). C is the equivalent capacitance of the capacitor (F). τ is time
165 constant (s) which can be expressed by functions of the activation overvoltage and the
166 concentration overvoltage as shown in Equation (9) [37]:

167 $$\tau = C(R_{\mathrm{act}} + R_{\mathrm{con}}) = \frac{C(V_{\mathrm{act}}+V_{\mathrm{con}})}{I} \tag{9}$$

168 Where, R_{con} is the concentration equivalent resistance and R_{act} is the activation
169 equivalent resistance as shown in Fig. 1 (b).

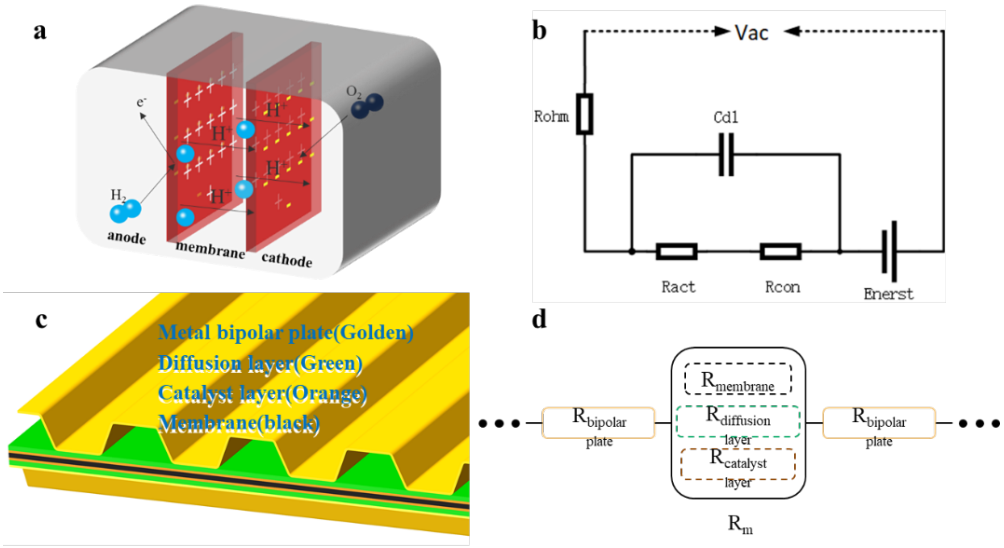

171 Fig. 1. (a) and (b) Charge double layer and equivalent circuit model of PEMFC; (c)
172 Cross-sectional picture of single cell; (d) Heat transfer equivalent circuit.

2.1.2. Reactant flow model

Reactant flow model is developed for determining the effective partial pressure of hydrogen and oxygen at the anode and cathode [27, 28]. The reactant flow model is established on the ideal gas law and the principle of molar conservation. Reactant flow at any instant is equal to the gas inlet flow rate minus gas outlet flow rate and gas consumption. The anode gas pressure can be calculated using Equation (10):

$$\begin{aligned} \frac{V_{\mathrm{a}}}{RT}\frac{dP_{\mathrm{H_2}}}{dt} &= \dot{m}_{\mathrm{H_2,in}} - \dot{m}_{\mathrm{H_2,out}} - \dot{m}_{\mathrm{H_2,used}} \\ \dot{m}_{\mathrm{H_2,out}} &= k_{\mathrm{a}}(P_{\mathrm{H_2}} - P_{\mathrm{tank}}) \end{aligned} \tag{10}$$

Where V_{a} is anode volume (m^3), $\dot{m}_{\mathrm{H_2,in}}$ and $\dot{m}_{\mathrm{H_2,out}}$ are hydrogen inlet and outlet flow rate ($mol \cdot s^{-1}$), respectively. $\dot{m}_{\mathrm{H_2,out}}$ is related to hydrogen pressure at the inlet and anode flow constant ka (mol·s-1bar-1). $\dot{m}_{\mathrm{H_2,used}}$ is the total hydrogen usage ($mol \cdot s^{-1}$) which is related to the cell numbers and stack current. Parameters of the electrochemical model are presented in Table 1. The air-cooled PEMFC stack is assembled by metallic bipolar plates that made of 316L stainless steel.

Table 1: Parameters of the electrochemical model

Parameter	Value	Units
Number of cells N	50	N/A
Hydrogen pressure	1.5	bar
Cell area A	100	cm^2
Anode volume V_{a}	0.0025	m^3
Cathode volume V_{c}	0.0025	m^3

Anode flow constant	0.065	$mol \cdot s^{-1} bar^{-1}$
Cathode flow constant	0.065	$mol \cdot s^{-1} bar^{-1}$

2.2. Thermal model

Fig. 2 presents the thermal balance within the air-cooled PEMFC stack, there are mainly two parts: membrane electrode assembly (MEA) and metallic bipolar plate (made of 316L stainless steel). The MEA is considered as heat source, the thermal energy is transferred to bipolar plates by heat conduction and air by convection. In this study, the excess hydrogen is re-circulated to the anode, hydrogen flow is much less than air flow, Therefore the heat exchange with hydrogen can be ignored. The thermal model is lumped model and the temperature gradients between the inlet and the outlet of each cell is neglected. As shown in Fig. 1, only in the gas channels, the MEA (GDL) and the metallic bipolar plate contact with ambient air. Therefore, heat loss to the air will occur in these surfaces. The thermal balance within the MEA of the stack can be calculated using Equation (11):

$$C_{\mathrm{M}} \frac{dT}{dt} = P_{\mathrm{tot}} - P_{\mathrm{elec}} - q_{\mathrm{M,mbp}} - q_{\mathrm{M,a,loss}} \tag{11}$$

Where, T is the stack temperature (K). C_{M} is the thermal capacitance ($J \cdot K^{-1}$). P_{elec} is the cell electrical power output (W) which equals to $V_{\mathrm{Cell}} I_{\mathrm{cell}}$. $q_{\mathrm{M,mbp}}$ is the heat flow through the MEA surface to the metallic bipolar plate (W). $q_{\mathrm{M,a}}$ is the heat flow from the MEA to the air flowing in the gas channel (W). P_{tot} is the total power input (W) which can be calculated using Equation (12):

$$P_{\mathrm{tot}} = \frac{NI_{\mathrm{cell}}}{2F}\Delta H \tag{12}$$

Where, ΔH is the enthalpy of oxidation for the hydrogen (285.5 KJ·mol^{-1}). F is the Faraday constant (96,485 C·mol^{-1}). The thermal balance of the metallic bipolar plate can be calculated using Equation (13):

$$C_{\mathrm{mbp}}\frac{dT_{\mathrm{mbp}}}{dt} = q_{\mathrm{M,mbp}} - q_{\mathrm{mbp,a}} \tag{13}$$

Where T_{mbp} is the metallic bipolar plate temperature (K). C_{mbp} is thermal capacitance (J·K^{-1}). $q_{\mathrm{mbp,a,loss}}$ is the heat loss to the air from the metallic bipolar plate (W).

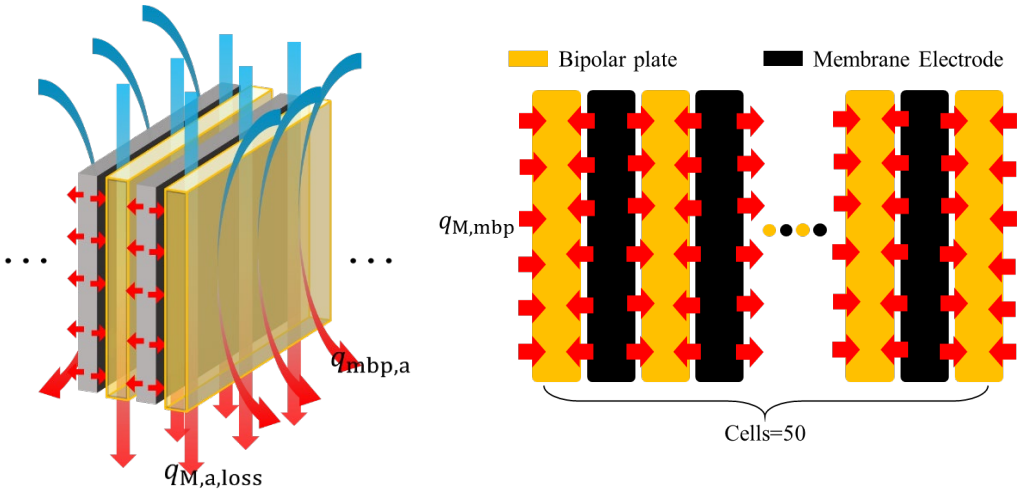

Fig. 2. Thermal balance of PEMFC stack applied with metallic bipolar plate.

In Equation (11) and (13), the heat transfer $q_{\mathrm{M,mbp}}$ can be calculated as $\frac{T-T_{\mathrm{mbp}}}{R_{\mathrm{M}}}$; $q_{\mathrm{M,a,loss}}$ can be calculated as $\frac{T-T_{\mathrm{amb}}}{R_{\mathrm{M,a}}}$ and $q_{\mathrm{mbp,a}}$ can be calculated as $\frac{T_{\mathrm{mbp}}-T_{\mathrm{amb}}}{R_{\mathrm{mbp,a}}}$. T_{amb} is the ambient temperature (K). Thermal resistance of the MEA R_{M} (K·W^{-1}), thermal resistance between the MEA and the surrounding air $R_{\mathrm{M,a}}$ (K·W^{-1}) and thermal resistance between the metallic bipolar plate and the surrounding air $R_{\mathrm{mbp,a}}$ (K·W^{-1}) can be expressed as shown in Equation (14) – (15). The thermal resistance of

the MEA is the summation of thermal resistance of the membrane, the catalyst layers and the gas diffusion layers:

$$R_{\mathrm{M,mbp}} = \frac{\delta_{\mathrm{m}}}{\kappa_{\mathrm{m}} \times A_{\mathrm{m}}} + \frac{\delta_{\mathrm{cl}}}{\kappa_{\mathrm{cl}} \times A_{\mathrm{cl}}} + \frac{\delta_{\mathrm{gdl}}}{\kappa_{\mathrm{gdl}} \times A_{\mathrm{gdl}}} + \frac{\delta_{\mathrm{mbp}}}{\kappa_{\mathrm{mbp}} \times A_{\mathrm{mbp}}} \quad (14)$$

$$R_{\mathrm{M,a}} = \frac{1}{h_{\mathrm{M,a}} \times A_{\mathrm{M}}} \quad (15)$$

$$R_{\mathrm{mbp,a}} = \frac{1}{h_{\mathrm{mbp,a}} \times A_{\mathrm{mbp}}} \quad (16)$$

Where, k_{m} is the thermal conductivity of the membrane ($\mathrm{W \cdot m^{-1} K^{-1}}$). A_{m} is the area of the membrane ($\mathrm{m^2}$). δ_{m} is the membrane thickness (m). k_{cl} is the thermal conductivity of the catalyst layer ($\mathrm{W \cdot m^{-1} K^{-1}}$). A_{cl} is the area of the catalyst layer ($\mathrm{m^2}$). δ_{cl} is the catalyst layer thickness (m). k_{gdl} is the thermal conductivity of the gas diffusion layer ($\mathrm{W \cdot m^{-1} K^{-1}}$). A_{gdl} is the area of the gas diffusion layer ($\mathrm{m^2}$). δ_{gdl} is the gas diffusion layer thickness (m). δ_{mbp} is the metallic bipolar plate thickness (m), k_{mbp} is the thermal conductivity of the metallic bipolar plate ($\mathrm{W \cdot m^{-1} K^{-1}}$). A_{M} is the area of the MEA ($\mathrm{m^2}$). A_{mbp} is the area of the metallic bipolar plate ($\mathrm{m^2}$). $h_{\mathrm{M,a}}$ is the convective heat transfer coefficient of the MEA to the surrounding air ($\mathrm{W \cdot m^{-2} K^{-1}}$). $h_{\mathrm{mbp,a}}$ is the convective heat transfer coefficient of the metallic bipolar plate to the surrounding air ($\mathrm{W \cdot m^{-2} K^{-1}}$). For the air-cooled PEMFC stack, fan supplies cathode intake air, meanwhile, the air flow removes waste heat to maintain thermal balance for the PEMFC stack. Both $h_{\mathrm{M,a}}$ and $h_{\mathrm{mbp,a}}$ are function of air stoichiometric (or air flow rate). In other words, the air stoichiometric is expected to impact on the cooling capacity and thermal imbalance of the PEMFC stack. This will be investigated and discussed later in more details.

2.3. Environmental model

The ambient temperature and oxygen partial pressure varies with altitude which greatly affect the performance of the stack. According to the International Standard Atmosphere (ISA) model [40, 41], the variation of atmospheric temperature T_{atmo} (K) and atmospheric pressure P_{atmo} (bar) with altitude is given as follow Equations (17) and (18):

$$T_{\mathrm{atmo}} = T_0 - 6.5 \times h_L \tag{17}$$

Where, h_{L} is the altitude (km). T_0 is the air temperature at sea level (K).

$$P_{\mathrm{atmo}} = P_0 \left[1 - \left(6.5 \times \frac{h_{\mathrm{L}}}{T_0}\right)\right]^{5.2561} \tag{18}$$

Where, P_0 is the air pressure at sea level (K). Parameters of the MEA consists of membrane, catalyst layers and gas diffusion layers and the metallic bipolar plates are shown in Table 2.

Table 2: Parameters of the thermal model

Parameter	Value	Units
Membrane thickness δ_{m}	0.02	mm
Catalysts layers thickness δ_{cl}	0.01	mm
Gas diffusion layers thickness δ_{gdl}	0.02	mm
Metallic bipolar plate thickness δ_{mbp}	1.00	mm
Thermal conductivity of membrane k_{M}	0.67	$W \cdot m^{-1}K^{-1}$
Thermal conductivity of catalyst layer k_{cl}	8	$W \cdot m^{-1}K^{-1}$

Thermal conductivity of gas diffusion layer k_{gdl}	1.6	$\mathrm{W{\cdot}m^{-1}K^{-1}}$
Thermal conductivity of metallic bipolar plate k_{mbp}	16.2	$\mathrm{W{\cdot}m^{-1}K^{-1}}$

3. Results and discussions

3.1. Model validation

The predicted polarization curve is compared to the experimental data from Ref. [25]. As shown in Fig. 3, the generally good fit to the experimental data confirms the model is reliable (the average error is below 0.5%). It should be noted that this current density range is representative of common steady-state operating conditions [25]. The number of cells, the cell area is 50 and 100 $\mathrm{cm^2}$ respectively and the operation conditions are shown in Fig. 3. Since the influence on losses of porous media microstructure, of cell water uptake and of lack of precise reactant gases distribution at the cathode side at high current density (over 0.8 $\mathrm{A{\cdot}cm^{-2}}$), the error between model and experimental data is less satisfactory. These microstructure features are not properly accounted for in the present modeling.

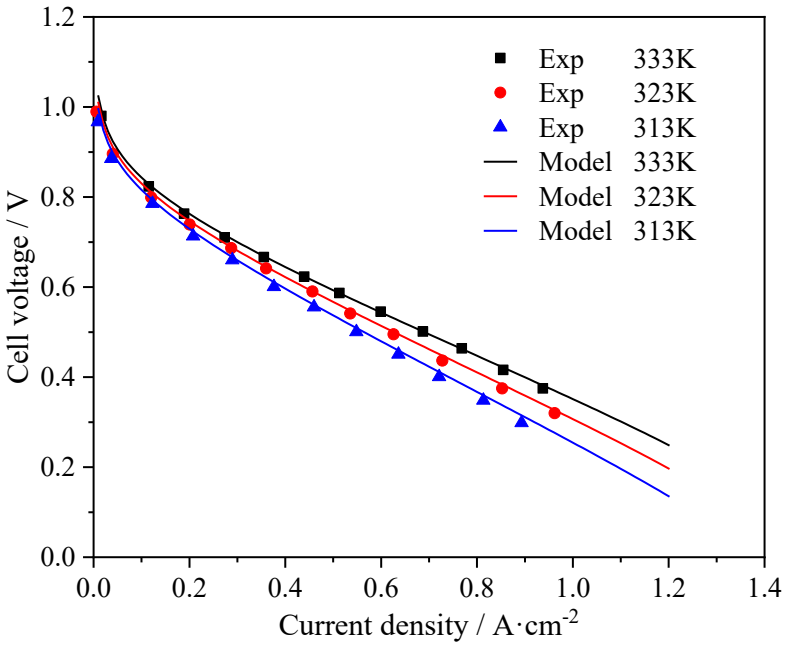

Fig. 3. Polarization curve – comparison of PEMFC electrochemical model results and experimental data

3.2. Impact of altitude variations

3.2.1. Stack voltage and current density

During the flight missions, altitude variations lead to changes in the atmospheric temperature and pressure, have significant impact on the stack performance and bring great challenges for the thermal management as well. It will also affect the individual cell voltages and temperatures within the stack. The calculation results of dynamic characteristics will be described in the following sections.

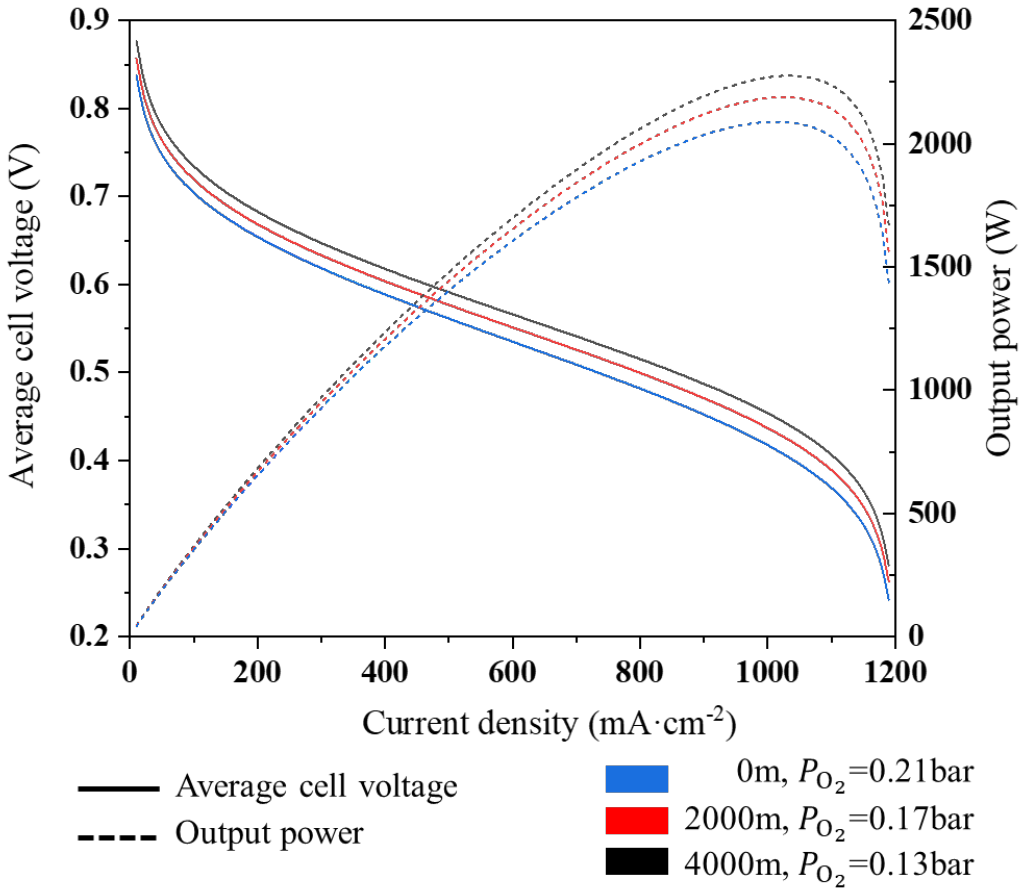

278 Fig. 4. Air-cooled PEMFC cell voltage and power output varies with current density
279 at different altitudes (simulation results).

280 Fig. 4 presents the cell voltage and stack power output variations with the current
281 density at different altitudes of 0m, 2000m and 4000m. At the current density of 400
282 mA·cm^{-2}, the output electric power decreases from 1,236W to 1,178W with altitude
283 increases from 0m to 4000m, the decline rate is 4.7%. This value is 6.5% at the current
284 density of 800 mA·cm^{-2}, from 2269W to 1972W. As presented in Equation (17), altitude
285 increment leads to decrease in the atmospheric pressure, so as the oxygen partial
286 pressure, this results in the stack power loss and stack performance decrease. The
287 performance degradation of the PEMFC stack responding to the altitude variations is

relatively more serious at the high current density.

As shown in Fig. 5 (a), at the sea level (altitude = 0m), the stack voltage drops from 32.0 V and gradually rises to 29.8 V when the current density increases from 400 $mA \cdot cm^{-2}$ to 600 $mA \cdot cm^{-2}$. The voltage reaches stability around 200s due to the thermal balance between the stack and the air flow in the gas channels. In addition, it takes longer before the voltage reaches stability at low altitude (about 20-50s). This because the ambient temperature is higher at low altitude, the stack will stabilize at a higher temperature.

Fig. 5 (b) presents the dynamic response of the stack voltage to the change in altitude (from 0 m to 2000 m during the time of 1000-1100s and from 2000 m to 4000 m during the time of 2000-2100) at the same operating current. The voltage does not change suddenly with the change of altitude, but has a certain delay, and the change is more smooth. Since the stack temperature decreases with the increase of altitude as mentioned before, the voltage decreases slowly with the altitude and reaches stability within 100s after the altitude stabilizes. When the current density is 400 $mA \cdot cm^{-2}$, the stack voltage is 32.0 V at the altitude of 0 m, it drops to about 31.5 V at the altitude of 2000 m, the decline is 0.16%. When the altitude varies from 2000 m to 4000 m, the decline will be less than 0.16%. Overall, stack voltage drop as altitude increases is quite small about 0.25 $V \cdot km^{-1}$ (5E-3$V \cdot km^{-1}$ for cell voltage). The impact of the current density on the stack voltage is 1.2 V per 100 $mA \cdot cm^{-2}$ variation.

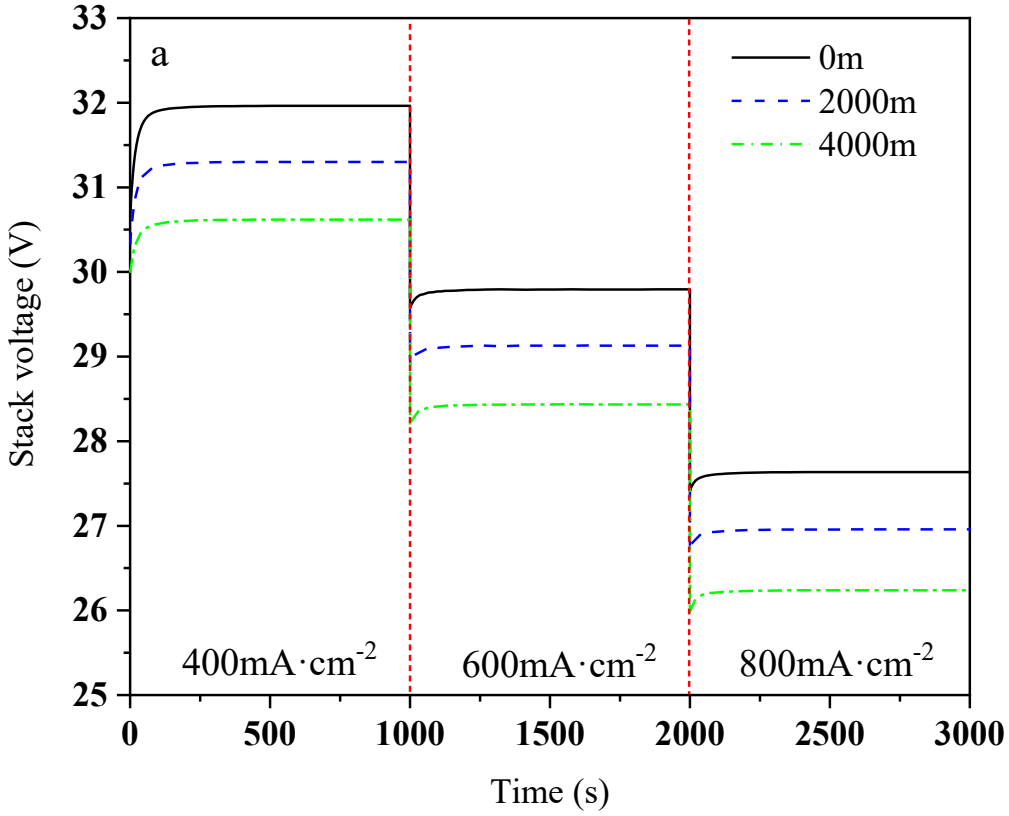
a
0m
2000m
4000m
Stack voltage (V)
Time (s)
400mA·cm-2
600mA·cm-2
800mA·cm-2
33
32
31
30
29
28
27
26
25
0
500
1000
1500
2000
2500
3000

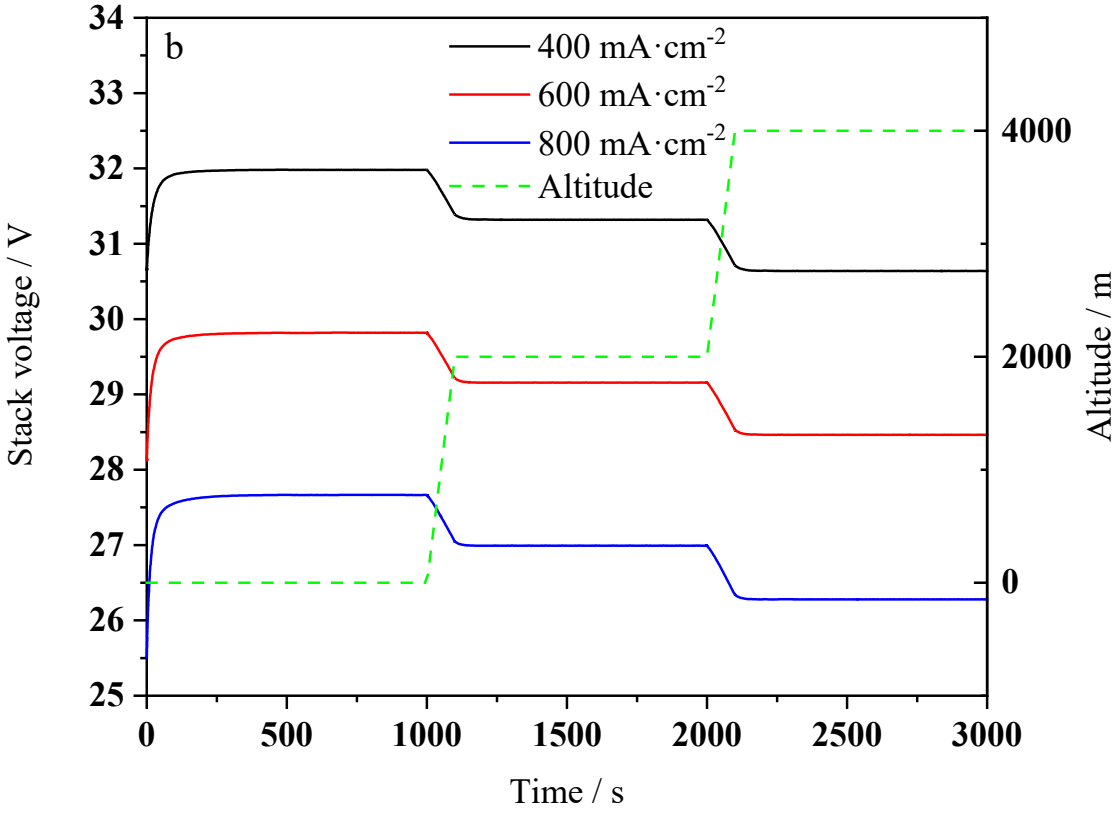
b
400 mA·cm-2
600 mA·cm-2
800 mA·cm-2
Altitude
Stack voltage / V
Altitude / m
Time / s
34
33
32
31
30
29
28
27
26
25
4000
2000
0
0
500
1000
1500
2000
2500
3000

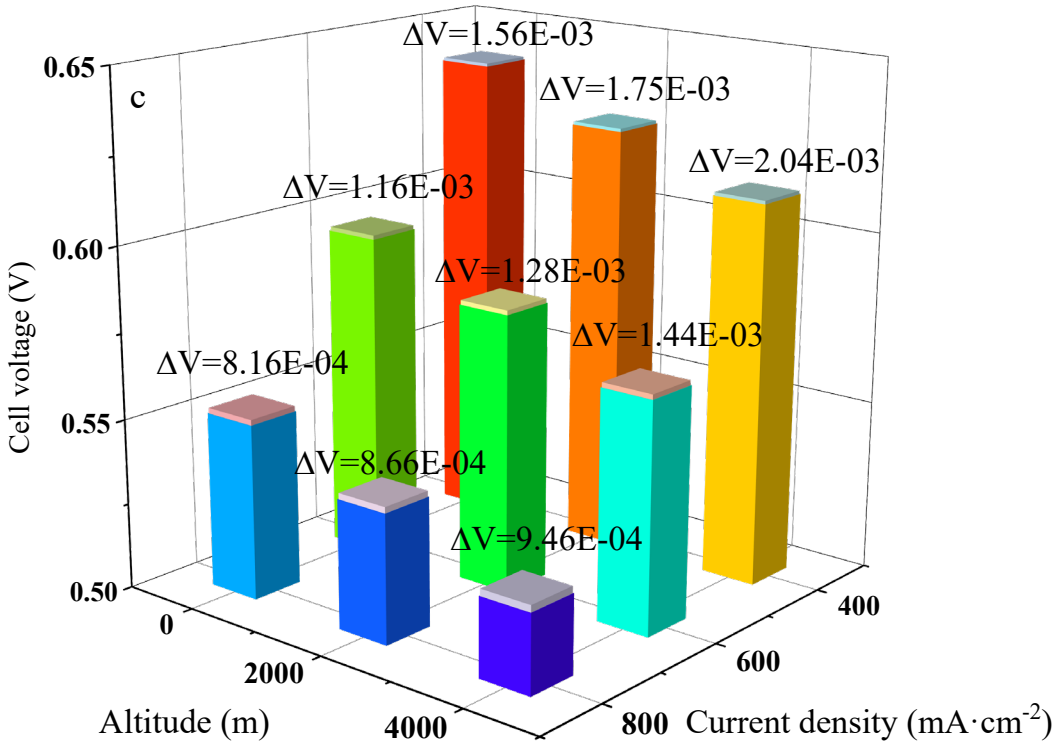

311 Fig. 5: (a) Dynamic response of stack voltage to the current density step change at
312 different altitudes (0 m, 2000 m and 4000 m); (b) Dynamic response of stack voltage
313 to the altitude change at different current density (400 mA·cm^{-2}, 600 mA·cm^{-2}, 800
314 mA·cm^{-2}); (c) Cell voltage and voltage differences under different current densities
315 (400, 600 and 800 mA·cm^{-2}) and different altitudes (0 m, 2000 m and 4000 m).

316 In the PEMFC stack, each cell will output different voltage, the voltage distribution is
317 parabolic and symmetrical, the cell voltage is higher at the center and lower at the side.
318 Fig. 5 (c) presents the cell voltage and the largest cell voltage difference under different
319 current densities (400, 600 and 800 mA·cm^{-2}) and different altitudes (0 m, 2000 m and
320 4000 m). Cell voltage decreases as altitude increases or as current density increases. At
321 the altitude of 0 m, the difference between the highest and lowest voltages are 8.16E-

04, 1.16E-03 and 1.56E-03V at the current density of 400, 600 and 800 $mA \cdot cm^{-2}$ respectively. When the altitude reached 4000m, the largest voltages are 9.49E-04, 1.44E-03 and 2.04E-03V respectively. The cell voltage distribution is slightly less homogeneous as altitude increases or as current density decreases.

3.2.2. Cell temperature distribution

The PEMFC operating temperature and temperature difference are critical. Too high operating temperature leads to dehydration and even rupture of the membrane. Fig. 6 (a), (b) and (c) present the cell temperature distribution when current densities step change at altitudes 0, 2000 and 4000 m. The stack could be considered as an assemble of many plates containing internal heat sources, the fuel cell temperature distribution is 'symmetric parabola' as shown in Fig. 6. More details of the cell temperature distribution and temperature differences have been summarized and presented in Fig. 6 (d). As shown in Fig. 6 (d), the cell temperature increases with increasing current density or with decreasing altitude. At the altitude of 0m, the operating temperature is 325K when the current density is at 800 $mA \cdot cm^{-2}$. At the altitude 4000 m, the operating temperature drop to 300K at the same current density. At the lower altitude, the atmospheric temperature is relatively higher, the difference of stack or cell temperature with surrounding air decreases, this makes it extremely challenging for thermal management.

As shown in Fig. 6 (d), the air-cooled PEMFC stack applied with metallic bipolar plate demonstrates a largest cell temperature difference of about 1.9 K (or ºC) at the current

density of 400 mA·cm^{-2} and the altitude of 0 m. The largest temperature difference within the stack increases from 1.9 to 2.8 and 3.7 K when the current density increases from 400, to 600 and 800 mA·cm^{-2}. The temperature difference increases significantly with the increasing current density. The largest cell temperature difference barely changes when the altitude varies from 0 m to 2000 m or 4000 m.

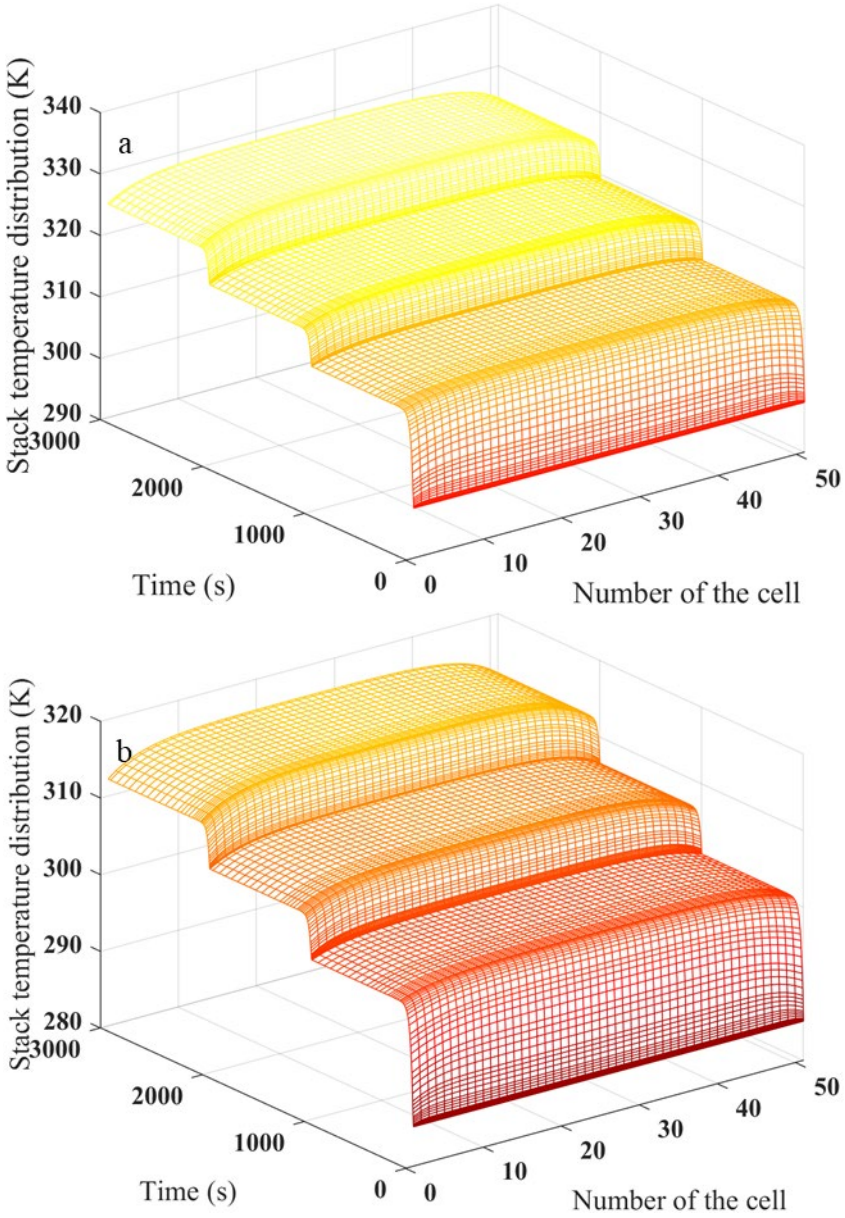

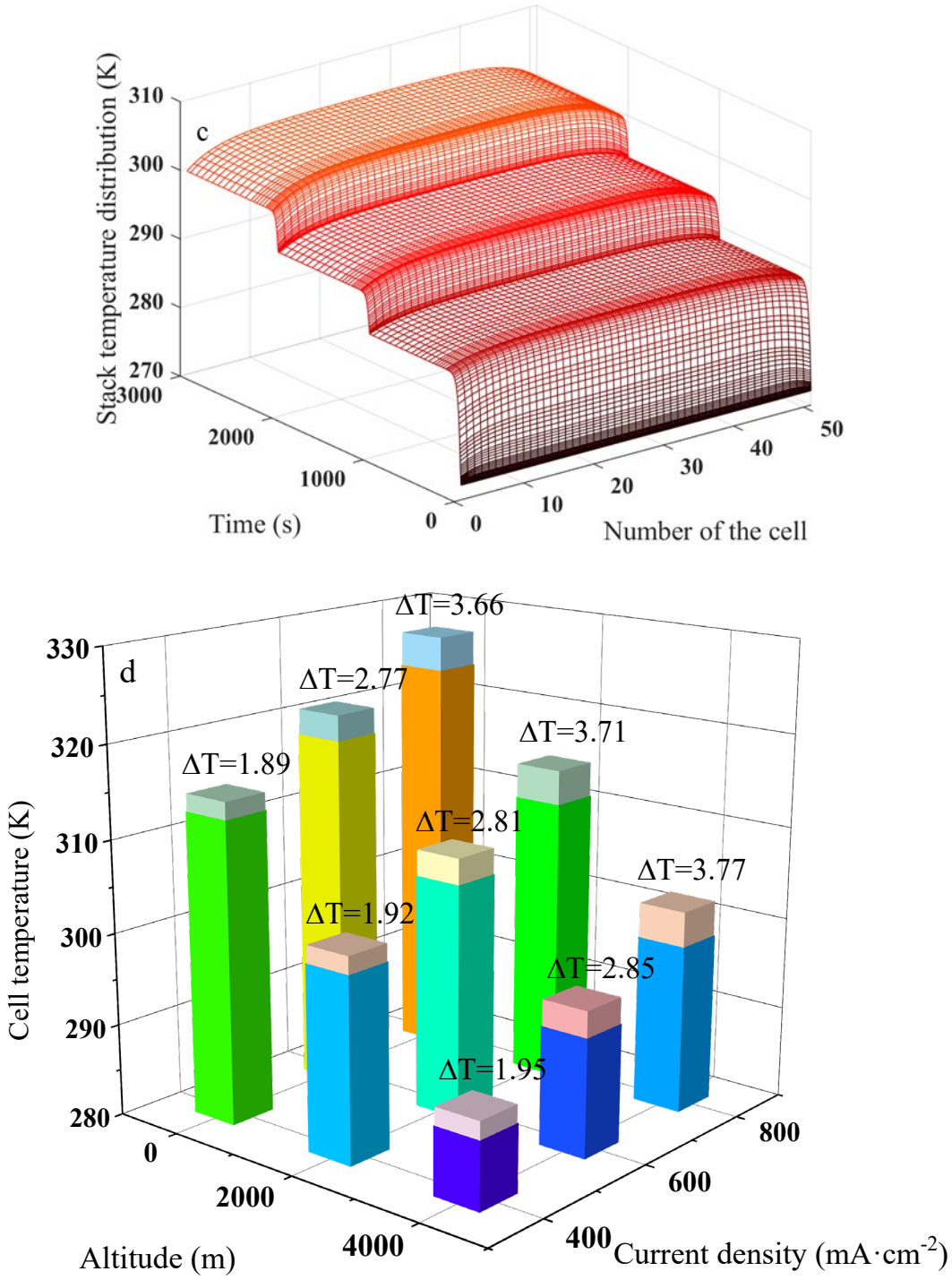

352 Fig. 6. Temperature distribution when current densities step changed at altitudes (a) 0m;

353 (b) 2000m; (c) 4000m; (d) cell temperature difference.

354 **3.3. Impact of air stoichiometric ratio**

The altitude variations during the flight mission impact on the stack performance and thermal management. For the air-cooled PEMFC stack, fan supplies cathode intake air, meanwhile, the air flow removes waste heat to maintain thermal balance. The air flow is used to ensure the sufficient reactant oxygen and for cooling purpose. The stack power output and thermal power are both functions of the air stoichiometric ratio. It is possible to regulate the air stoichiometric ratio for controlling stack power output and operating temperature to compensate certain impact of the altitude variations.

3.3.1. Stack thermal power and temperature

Fig. 7 (a), (b) and (c) present the impact of the air stoichiometric ratio variations (stoic. = 100, 150 and 200) on heat power, heat exchange rate and stack temperature at three different current density (400 $mA \cdot cm^{-2}$, 600 $mA \cdot cm^{-2}$ and 800 $mA \cdot cm^{-2}$) and the altitude of 0m. As shown in Fig. 7 (a), the current density is 400 $mA \cdot cm^{-2}$, thermal power and heat exchange rate stay almost the same after 150s and the results stabilizes to around 1670 W independent of the air stoichiometric ratio. The stack operating temperature decreases from 318.6 K to 316.0 K and to 314.4 K when the air stoichiometric ratio increases from 100 to 150 and to 200.

As shown in Fig. 7 (c), the stack temperature reached 333.9 K at the current density of 800 $mA \cdot cm^{-2}$ and a stoichiometric ratio of 100. Comparing Fig. 7 (a), (b) and (c), at the air stoichiometric ratio of 100, the thermal power increases from 1670 W to 2650 W and to 3700 W, the stack temperature increases from 318.6 K to 326.3 K and to 333.9 K when the current density increases. Increasing the air stoichiometric ratio barely

affects the stack thermal power, but help decreasing the stack temperature.

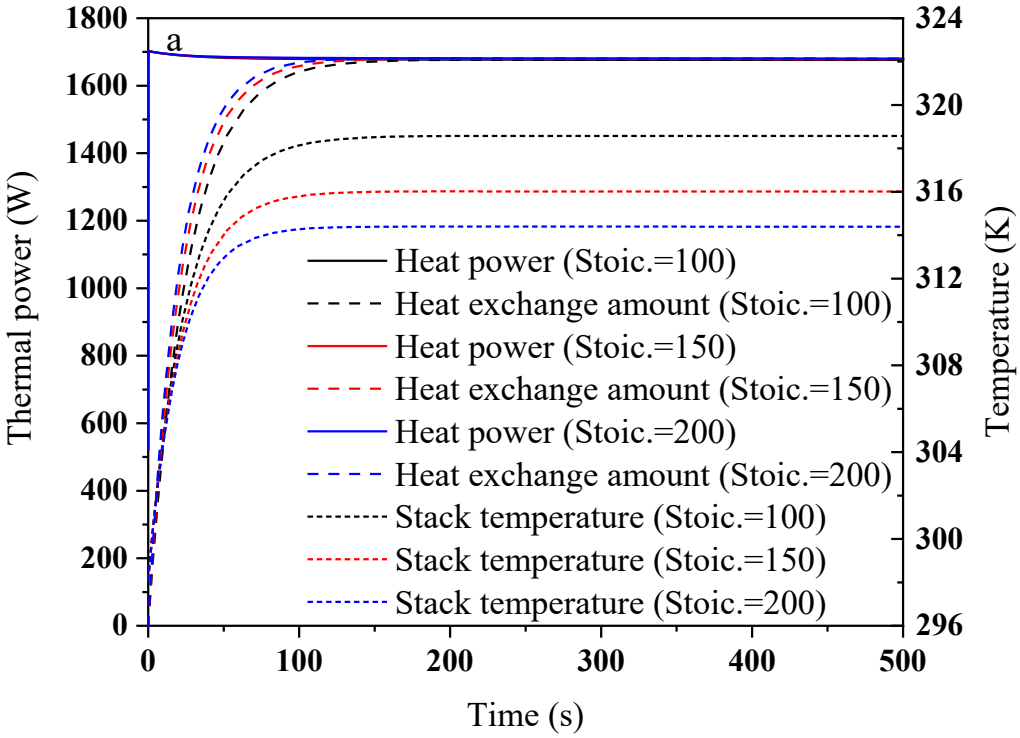

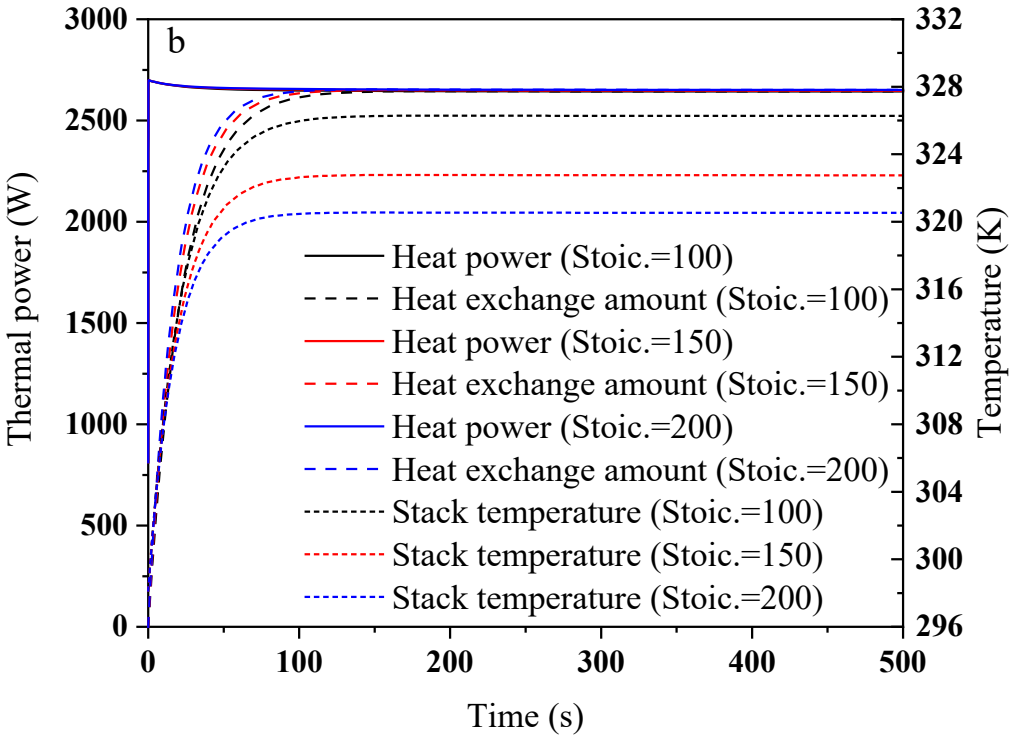

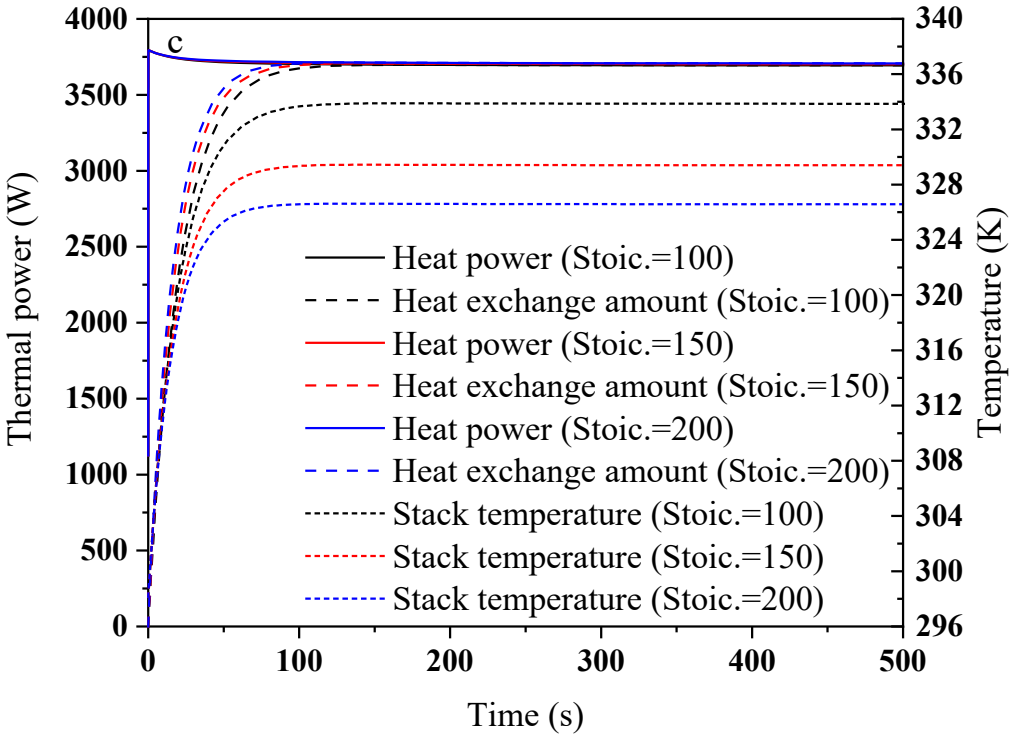

380 Fig. 7. Thermal power and stack temperature at altitude of 0 m and at various current

density (a) 400 mA·cm^{-2} (b) 600 mA·cm^{-2} (c) 800 mA·cm^{-2}

3.3.2. Stack power output and temperature

When the air stoichiometric ratio increases, Reynolds number, Nusselt number and convective heat transfer coefficient increase which enhance the cooling heat transfer, thus the stack temperature decreases. Fig. 8 presents the stack temperature and power output at different current density when air stoichiometric ratio increases at the altitude of 0m (298K). At current density 400 mA·cm^{-2}, the effect of air stoichiometric ratio on temperature reduction decreases as the ratio increases. The air stoichiometric ratio variations mainly impact on stack temperature, barely impact on stack power output. When the current density varies from 400 mA·cm^{-2} to 600 mA·cm^{-2} and to 800 mA·cm^{-2}, the stack power output increases from 1260 W to 1760 W and to 2180 W and the stack temperature increases from 323.0 K to 342.2 K.

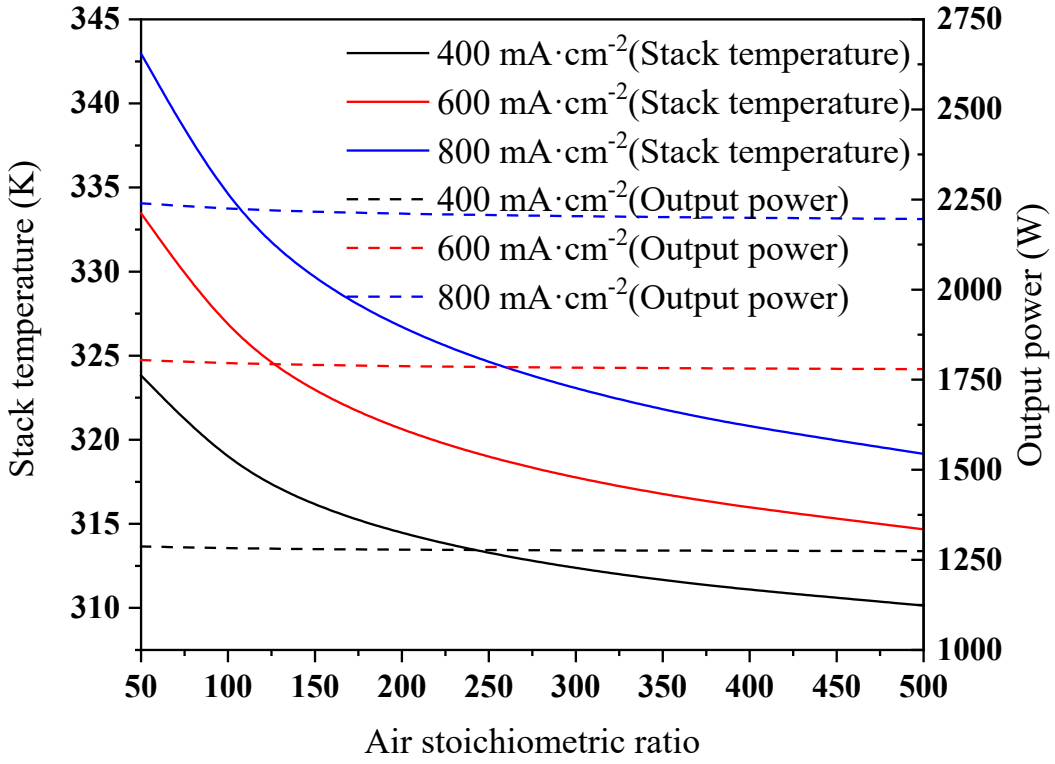

394 Fig. 8. Stack temperature and power output at different current density (400, 600 and

395 800 mA·cm^{-2})

396 **3.3.3. Minimum air stoichiometric ratio**

397 To avoid severe stack degradation, the maximum stack operating temperature is set as

398 333 K. According to temperature limitation, the minimum required air stoichiometric

399 ratio at the current density range of 400 to 800 mA·cm^{-2} and at different altitude has

400 been shown in Fig. 9. If the air stoichiometric ratio stays constant, the maximum current

401 density for operation at different altitudes can be found as well according to Fig. 9.

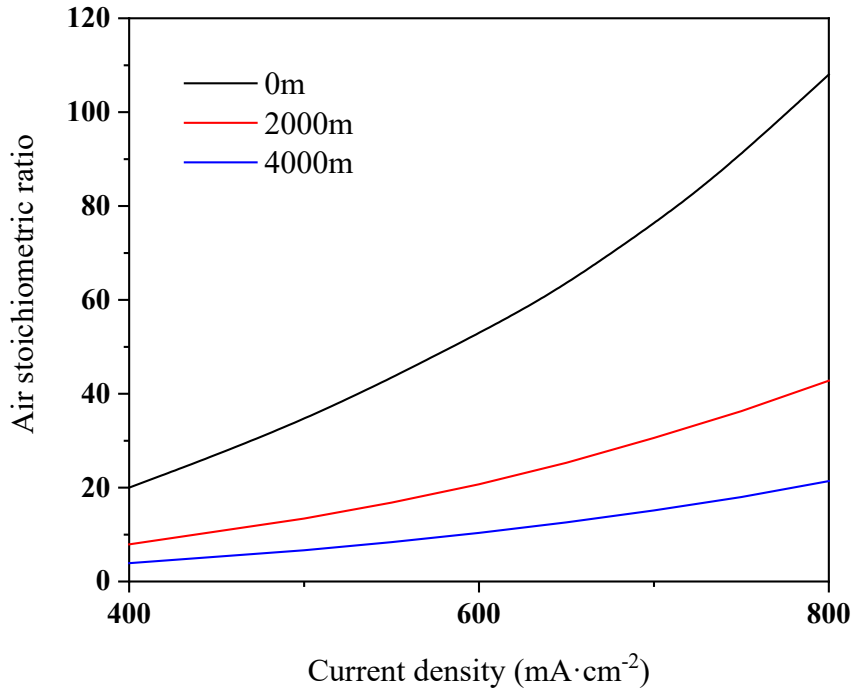

403 Fig. 9. Minimum required air stoichiometric ratio at different altitudes (0 m, 2000 m
404 and 4000 m)

405 The minimum required air stoichiometric ratio at the current density of 400 mA·cm^{-2} is
406 20. When the current density is 800 mA·cm^{-2}, the air stoichiometric ratio should be at
407 least 108. According to the Eq. (17), the ambient temperature decreases with the
408 increasing altitude (Fig. 6(d)). More energy is converted into thermal energy at lower
409 temperature under the same current density (Fig. 5(c)). In this turn, larger air
410 stoichiometric ratio is needed to satisfy the stack cooling demand. However, the
411 increase of heat exchange temperature difference caused by the lower ambient
412 temperature makes a significant improvement of heat exchange capacity. Therefore, the
413 minimal air stoichiometric ratio is lower at the higher altitude. At the same altitude of

0 m, when current density increases, more energy is converted into thermal energy at high current density, a higher air stoichiometric ratio is needed to enhance the cooling capacity. Therefore, minimum required air stoichiometric ratio is larger at high current density.

When the altitude increases to 2000m, atmospheric temperature reduces by 12 K (°C) for the studied case, which leads to the increase of temperature difference between the PEMFC stack and the surrounding air, so a smaller air stoichiometric ratio will be required. Fig. 9 shows that at the current density of 400 $mA \cdot cm^{-2}$, the minimum required air stoichiometric ratio is 20 at the altitude of 0 m, this requirement decreases to 8 when the altitude increases to 2000 m, it reduces to 4 when the altitude increases to 4000m. At the current density of 800 $mA \cdot cm^{-2}$, the minimum required ratio decreases from 110 to 22 when the altitude increases to 4000m.

4. Conclusions

In this paper, a dynamic coupled electrochemical and thermal model for the air-cooled PEMFC used in UAV is proposed. The impact of the metallic bipolar plate on the stack thermal balance is considered; an environmental model estimating atmospheric temperature and pressure variations with altitude is included. Influences of altitude variations and air stoichiometric ratio on stack operational performance and thermal management are studied. The main conclusions for this study are as follows:

a. With altitude increases from 0 to 4000 m, the output electric power decline is 4.7-6.5% at the current density of 400-800 $mA \cdot cm^{-2}$. The power loss of the stack due to the

435 altitude increment is larger at the high current density regime. The stack voltage drop
436 is 0.25 $V \cdot km^{-1}$ (5E-3$V \cdot km^{-1}$ for cell voltage) when altitude increases.
437 b. At sea level, the stack operating temperature increases to 325K at the current density
438 of 800 $mA \cdot cm^{-2}$; it is more challenging for the stack thermal management. The
439 temperature difference of cells in the stack barely change when altitude varies from 0
440 to 4000 m, it stays 3.8K at current density of 800 $mA \cdot cm^{-2}$.
441 c. To avoid severe stack degradation due to high stack temperature, a minimum air
442 stoichiometric ratio is required for maintaining stack thermal balance. When the altitude
443 increases from 0 to 4000m, the minimum required air stoichiometric ratio decreases
444 from 110 to 22 at the current density of 800 $mA \cdot cm^{-2}$.

445 **Acknowledgements**

446 This study was supported bythe National Key Research and Development Program of
447 China, the National Natural Science Foundation of China (Nos. 51776144, 52076096),
448 Natural Science Foundation of Hubei Province (No. 2020CFA040) and Wuhan Applied
449 Foundational Frontier Project (No. 2020010601012205).

450 **References**

451 [1] X. Lü, Y. Qu, Y. Wang, C. Qin, G. Liu, A comprehensive review on hybrid power
452 system for PEMFC-HEV: Issues and strategies, Energ Convers Manage
453 171(2018) 1273-1291.
454 [2] C. Gong, J. Shen, Y. Yu, K. Wang, Z. Tu, A novel radiator structure for enhanced
455 heat transfer used in PEM fuel cell vehicle, Int J Heat Mass Tran 157(2020)

119926.

[3] M. Bornapour, R. Hooshmand, M. Parastegari, An efficient scenario-based stochastic programming method for optimal scheduling of CHP-PEMFC, WT, PV and hydrogen storage units in micro grids, Renew Energ 130(2019) 1049-1066.

[4] H. Chang, C. Duan, X. Xu, H. Pei, S. Shu, Z. Tu, Technical performance analysis of a micro-combined cooling, heating and power system based on solar energy and high temperature PEMFC, Int J Hydrogen Energ 44(38)(2019) 21080-21089.

[5] N. Matulić, G. Radica, F. Barbir, S. Nižetić, Commercial vehicle auxiliary loads powered by PEM fuel cell, Int J Hydrogen Energ 44(20)(2019) 10082-10090.

[6] J. Shen, L. Xu, H. Chang, Z. Tu, S.H. Chan, Partial flooding and its effect on the performance of a proton exchange membrane fuel cell, Energ Convers Manage 207(2020) 112537.

[7] J. Shen, Z. Tu, S.H. Chan, Evaluation criterion of different flow field patterns in a proton exchange membrane fuel cell, Energ Convers Manage 213(2020) 112841.

[8] H. Fathabadi, Combining a proton exchange membrane fuel cell (PEMFC) stack with a Li-ion battery to supply the power needs of a hybrid electric vehicle, Renew Energ 130(2019) 714-724.

[9] A. Gong, D. Verstraete, Fuel cell propulsion in small fixed-wing unmanned aerial vehicles: Current status and research needs, Int J Hydrogen Energ 42(33)(2017)

21311-21333.

[10] J. Barroso, J. Renau, A. Lozano, J. Miralles, J. Martín, F. Sánchez, F. Barreras, Experimental determination of the heat transfer coefficient for the optimal design of the cooling system of a PEM fuel cell placed inside the fuselage of an UAV, Appl Therm Eng 89(2015) 1-10.

[11] N. Lee, J. Lee, S.W. Lee, S.S. Jang, H. Ju, Parametric study of passive air-cooled polymer electrolyte membrane fuel cell stacks, Int J Heat Mass Tran 156(2020) 119886.

[12] H. Wang, Stainless steel as bipolar plate material for polymer electrolyte membrane fuel cells, J Power Sources 115(2)(2003) 243-251.

[13] E. Özbek, G. Yalin, S. Ekici, T.H. Karakoc, Evaluation of design methodology, limitations, and iterations of a hydrogen fuelled hybrid fuel cell mini UAV, Energy 213(2020) 118757.

[14] K. Feng, Y. Shen, D. Liu, P.K. Chu, X. Cai, Ni–Cr Co-implanted 316L stainless steel as bipolar plate in polymer electrolyte membrane fuel cells, Int J Hydrogen Energ 35(2)(2010) 690-700.

[15] H. Tawfik, Y. Hung, D. Mahajan, Metal bipolar plates for PEM fuel cell—A review, J Power Sources 163(2)(2007) 755-767.

[16] F. Madadi, A. Rezaeian, H. Edris, M. Zhiani, Improving performance in PEMFC by applying different coatings to metallic bipolar plates, Mater Chem Phys 238(2019) 121911.

[17] J.L. Lu, N. Abbas, J.N. Tang, J. Tang, G.M. Zhu, Synthesis and characterization of conductive ceramic MAX-phase coatings for metal bipolar plates in simulated PEMFC environments, Corros Sci 158(2019) 108106.

[18] H. Fan, D. Shi, X. Wang, J. Luo, J. Zhang, Q. Li, Enhancing through-plane electrical conductivity by introducing Au microdots onto TiN coated metal bipolar plates of PEMFCs, Int J Hydrogen Energ 45(53)(2020) 29442-29448.

[19] S. Liu, T. Chen, Y. Xie, J. Zhang, C. Wu, Numerical simulation and experimental study on the effect of symmetric and asymmetric bionic flow channels on PEMFC performance under gravity, Int J Hydrogen Energ 44(56)(2019) 29618-29630.

[20] C. Zhao, S. Xing, M. Chen, W. Liu, H. Wang, Optimal design of cathode flow channel for air-cooled PEMFC with open cathode, Int J Hydrogen Energ 45(35)(2020) 17771-17781.

[21] S. Shimpalee, S. Greenway, J.W. Van Zee, The impact of channel path length on PEMFC flow-field design, J Power Sources 160(1)(2006) 398-406.

[22] B. Luo, M. Hu, F. Li, G. Cao, A novel material fabrication method for the PEM fuel cell bipolar plate, Int J Hydrogen Energ 35(7)(2010) 2643-2647.

[23] R. Taherian, 7 - Application of Polymer-Based Composites: Bipolar Plate of PEM Fuel Cells, In: R. Taherian, A. Kausar ds.), Electrical Conductivity in Polymer-Based Composites: William Andrew Publishing, 2019, pp. 183-237.

[24] R.F. Mann, J.C. Amphlett, M.A.I. Hooper, H.M. Jensen, B.A. Peppley, P.R.

519 Roberge, Development and application of a generalised steady-state
520 electrochemical model for a PEM fuel cell, J Power Sources 86(1)(2000) 173-
521 180.
522 [25] F. Musio, F. Tacchi, L. Omati, P. Gallo Stampino, G. Dotelli, S. Limonta, D.
523 Brivio, P. Grassini, PEMFC system simulation in MATLAB-Simulink®
524 environment, Int J Hydrogen Energ 36(13)(2011) 8045-8052.
525 [26] S.I. Seleem, H.M. Hasanien, A.A. El-Fergany, Equilibrium optimizer for
526 parameter extraction of a fuel cell dynamic model, Renew Energ 169(2021) 117-
527 128.
528 [27] M.J. Khan, M.T. Iqbal, Modelling and Analysis of Electro-chemical, Thermal,
529 and Reactant Flow Dynamics for a PEM Fuel Cell System, Fuel Cells 5(4)(2005)
530 463-475.
531 [28] Y. Qi, M. Espinoza-Andaluz, M. Thern, T. Li, M. Andersson, Dynamic
532 modelling and controlling strategy of polymer electrolyte fuel cells, Int J
533 Hydrogen Energ 45(54)(2020) 29718-29729.
534 [29] B. Zhang, F. Lin, C. Zhang, R. Liao, Y. Wang, Design and implementation of
535 model predictive control for an open-cathode fuel cell thermal management
536 system, Renew Energ 154(2020) 1014-1024.
537 [30] T.H. Oh, Conceptual design of small unmanned aerial vehicle with proton
538 exchange membrane fuel cell system for long endurance mission, Energ Convers
539 Manage 176(2018) 349-356.

[31] Z.U. Bayrak, U. Kaya, E. Oksuztepe, Investigation of PEMFC performance for cruising hybrid powered fixed-wing electric UAV in different temperatures, Int J Hydrogen Energ 45(11)(2020) 7036-7045.

[32] B. Wang, D. Zhao, W. Li, Z. Wang, Y. Huang, Y. You, S. Becker, Current technologies and challenges of applying fuel cell hybrid propulsion systems in unmanned aerial vehicles, Prog Aerosp Sci 116(2020) 100620.

[33] C. Depcik, T. Cassady, B. Collicott, S.P. Burugupally, X. Li, S.S. Alam, J.R. Arandia, J. Hobeck, Comparison of lithium ion Batteries, hydrogen fueled combustion Engines, and a hydrogen fuel cell in powering a small Unmanned Aerial Vehicle, Energ Convers Manage 207(2020) 112514.

[34] Ó. González-Espasandín, T.J. Leo, M.A. Raso, E. Navarro, Direct methanol fuel cell (DMFC) and H2 proton exchange membrane fuel (PEMFC/H2) cell performance under atmospheric flight conditions of Unmanned Aerial Vehicles, Renew Energ 130(2019) 762-773.

[35] J. Renau, J. Barroso, A. Lozano, A. Nueno, F. Sánchez, J. Martín, F. Barreras, Design and manufacture of a high-temperature PEMFC and its cooling system to power a lightweight UAV for a high altitude mission, Int J Hydrogen Energ 41(43)(2016) 19702-19712.

[36] T. Hordé, P. Achard, R. Metkemeijer, PEMFC application for aviation: Experimental and numerical study of sensitivity to altitude, Int J Hydrogen Energ 37(14)(2012) 10818-10829.

561 [37] J. Jia, Y. Wang, Q. Li, Y.T. Cham, M. Han, Modeling and Dynamic
562 Characteristic Simulation of a Proton Exchange Membrane Fuel Cell, IEEE T
563 Energy Conver 24(1)(2009) 283-291.
564 [38] T. Lan, K. Strunz, Modeling of multi-physics transients in PEM fuel cells using
565 equivalent circuits for consistent representation of electric, pneumatic, and
566 thermal quantities, Int J Elec Power 119(2020) 105803.
567 [39] J. Larminie, A. Dicks, M.S. McDonald, Fuel cell systems explained, J. Wiley
568 Chichester, UK, 2003.
569 [40] X. Song, L. Xin. Research on key technologies of standard atmosphere database.
570 2008 Asia Simulation Conference - 7th International Conference on System
571 Simulation and Scientific Computing2008. p. 1497-1500.
572 [41] S. Lee, R.C. Aldredge, Analytic approach to determine optimal conditions for
573 maximizing altitude of sounding rocket: Flight in standard atmosphere, Aerosp
574 Sci Technol 46(2015) 374-385.

575 **Nomenclature**

A	Area, cm^2
C	Thermal capacitance, $J \cdot K^{-1}$
E_{Nernst}	Nernst open circuit voltage, V
I	Current, A
k	Flow constant, $mol \cdot S^{-1}atm^{-1}$

m	Flow rate, $mol \cdot s^{-1}$
N	Number
P	Pressure, Pa
R	Circuit impedance, Ω
t	Time, s
T	Temperature, K
V	Volume, m^3
V_{cell}	Single cell voltage, V

Greek symbols

δ	Thickness, m
k	Thermal conductivity, $W \cdot m^{-1}K^{-1}$
υ	Overall voltage drop, V
τ	Time constant

Subscripts

a	Anode
act	Activation
atmo	Atmospheric
c	Contact resistances

ca	Cathode
cl	Catalyst layer
con	Concentration
d	Voltage drop
gdl	Gas diffusion layer
$H_{2,\ in}$	Hydrogen inlet
$H_{2,\ out}$	Hydrogen outlet
$H_{2,\ used}$	Total hydrogen usage
M	Membrane
mbp	Metallic bipolar plate
ohmic	Ohmic impedance

576

577